United Nations Educational, Scientific and Cultural Organization
GRÓ LRT Land Restoration Training Programme Under the auspices of UNESCO

GRÓ Land Restoration Training Programme
Árleynir 22, 112 Reykjavik, Iceland

Final project 2022

ESTIMATING ABOVEGROUND BIOMASS IN THE FOREST-STEPPE ZONE IN MONGOLIAN RANGELANDS USING SPECTRORADIOMETER AND REMOTE SENSING DATA

Dul Baatar
Agency for Land Administration and Management, Geodesy and Cartography
Government building XII, Barilgachdiin square, Chingeltei district
Ulaanbaatar, Mongolia
dul.b@gazar.gov.mn

Supervisor
Asra Salimi
Svarmi
asra@svarmi.com

ABSTRACT

Rangelands cover 70% of Mongolia and support forage for livestock and wildlife. Their aboveground biomass absorbs carbon and carries out photosynthesis, and the soil stores a large amount of carbon. Calculating aboveground biomass and mapping vegetation cover provides important background information for the implementation of rangeland management and using remote sensing for the biomass monitoring is crucial to save manpower, costs, and time. In this project, the aim was to develop a model to estimate aboveground biomass in the forest-steppe of Mongolia. This was done by analysing the relationship between the integrated data obtained from a Sentinel-2 Multispectral Instrument dataset, a ASD FieldSpec 4 Standard-Res portable spectroradiometer data, DJI Phantom 4 multispectral drone data and field sampling data, using the Random Forest algorithm. NDVI and MSAVI calculated from the Sentinel-2 Multispectral Instrument dataset and portable spectroradiometer data gave the best correlation with the field data and were thus used to develop the Random Forest model. Furthermore band 8 (NIR), band 4 (Red), band 3 (Green), and band 2 (Blue) of the Sentinel-2 Multispectral Instrument dataset were used for the Random Forest model. The Random Forest algorithm randomly selected 20% of all sampling data for testing and 80% of all sampling data for training in Python. The assessment, built on the Random Forest model results, are: RMSE = 36.3 kg/ha, RMSE% = 0.165, and R^2 = 0.94. I mapped the spatial distribution of predicted aboveground biomass in the test area using the Random Forest model. The study results showed that vegetation indices and spectral bands derived from the Sentinel-2 Multispectral Instrument dataset and portable

spectroradiometer data used in the Random Forest model have good potential for estimating aboveground biomass in the forest-steppe zone of Mongolia.

Key words: aboveground biomass, rangeland monitoring, vegetation index, Sentinel-2 MSI, spectroradiometer.

This paper should be cited as:

Baatar D (2022) Estimating aboveground biomass in the forest-steppe zone in Mongolian rangelands using spectroradiometer and remote sensing data. GRÓ Land Restoration Training Programme [Final project]
https://www.grocentre.is/static/gro/publication/848/document/baatar2022.pdf

TABLE OF CONTENTS

LIST OF FIGURES

LIST OF TABLES

ABBREVIATIONS

AGB	Aboveground biomass
ALAMGC	Agency for Land Administration and Management, Geodesy and Cartography
ASD	Analytical Spectral Device
DJI	Dà-Jiang Innovations
DVI	Different Vegetation Index
ESA	European Space Agency
EVI	Enhance Vegetation Index
FAO	Food and Agriculture Organizations of the United Nations
GEE	Google Earth Engine
MET	Minister of Environment and Tourism
MSAVI	Modified Soil Adjusted Vegetation Index
MSI	Multispectral Instrument
NAMEM	National Agency Meteorology and the Environmental Monitoring
NASA	National Aeronautics and Space Administration
NDVI	Normalization Different Vegetation Index
NIR	Near Infrared
NPP	Net Primary Productivity
RF	Random Forest algorithm
RS	Remote sensing
SDG	Sustainable Development Goals
SWIR	Short-Wave Infrared
UAV	Unmanned Aerial Vehicle
VI	Vegetation index
VNIR	Visible-Near Infrared

1. INTRODUCTION

Rangelands cover 54%, or approximately 79.5 million km^2, of the terrestrial land in the world (ILRI [International Livestock Research Institute] 2021) and supports forage for livestock and wildlife. Moreover, about two billion people are directly and indirectly dependent on rangelands worldwide (Thornton 2010). The available biomass of rangelands depends on net primary productivity (NPP) (Petz et al. 2014). The mean aboveground NPP of global rangelands is 1,017 Mg C/km^2 (Wolf et al. 2021). In rangeland, the aboveground biomass (AGB) absorbs carbon and carries out photosynthesis while the soil stores a large amount of carbon and prevents it from being released into the air. In recent decades, rangeland productivity has been negatively affected by climate change and overgrazing throughout the world (Godde et al. 2020).

The total territory of Mongolia is 1.56 million km^2, of which 70% (1.1 million km^2) is rangeland (ALAMGC [Agency for Land Administration and Management, Geodesy and Cartography] 2020). The livelihoods of more than 200,000 nomadic herder households are directly dependent on the rangelands for livestock production (Dagvadorj et al. 2013). Mongolian rangelands are vast and diverse and divided into six natural zones: alpine, mountain taiga, forest steppe, steppe, desert steppe, and desert (Gobi) (Yunatov 1976). The forest steppe is the one of the largest ecological zones in Mongolia, covering about 14.1% of the country, and provides the main natural resource for animal husbandry in Mongolia (Jigjidsuren & Johnson 2003).

Since 1990, the total number of livestock in Mongolia has increased constantly and tripled to about 90 million (Mongolian Statistical Information Service 2022). About 58% of rangelands are now altered or degraded because of overgrazing and climate change effects as reported in a recent report on rangeland health of Mongolia (Densambuu et al. 2018*a*). Due to the degradation, the amount of biomass and vegetation cover has been noticeably reduced. Therefore, the rangeland carrying capacity has been exceeded two to three fold, particularly in the forest steppe and steppe zone (Densambuu et al. 2018*b*). For this reason, it is crucial to have reliable biomass data throughout Mongolia. Based on accurate biomass estimations, land managers and herders could develop rangeland management plans every year. It would allow opportunities to use rangelands sustainably and to improve rangeland resilience and regenerative capacity. If sustainable management is successfully implemented, rangeland quality and forage production would improve and rangeland degradation would decrease (Densambuu et al. 2018*b*).

Since 2015, ALAMGC has been implementing the "Grazing land changes and grazing impact photo monitoring" project in cooperation with the Green Gold project, as part of its mandates pursuant to the Law on Land of Mongolia to introduce the rangeland use agreements and to establish a national monitoring network in every year (Dorj et al. 2021). Land managers conduct research on cover of plant functional groups, biomass, rangeland condition, and degradation level at 5,128 monitoring plots. In addition, the National Agency of Meteorology and the Environmental Monitoring (NAMEM) conducts national rangeland health monitoring at 1,516 monitoring plots yearly and collects more detailed vegetation data at plant species level (NAMEM and MEGDT [Ministry of Environment, Green Development and Tourism] 2015). To sum up these two monitoring systems, there are 20-30 monitoring plots in the territory of each *soum* (administrative division in Mongolia) (Dorj et al. 2021). Out of these 6,644 plots, about 1,800 monitoring plots are in the forest steppe zone. These rangeland monitoring systems are carried out by approximately 600 employees such as land officers and meteorologists, in the *soums* (ALAMGC 2020). These extensive rangeland monitoring systems are important but

costly with regard to budget, time and human resources. Therefore, it is also important to study large areas by remote sensing and, in particular to measure AGB on rangeland.

Due to the vast size of the Mongolian territory, diverse ecosystems, poor road system and lack of specialists, large amounts of labour and expenses are required to conduct nationwide monitoring and assessments in the field. Therefore, estimating AGB and mapping vegetation cover using remote sensing data is crucial to save manpower, costs, and time, as well as for providing important background information for rangeland management.

Remote sensing methods and technology have been developing since the early 1800s (Humboldt State University n.d.). At first, cameras were installed in air balloons and later on airplanes to gather images from the air. Now advanced techniques and technologies have been developed to observe the Earth's surface from space; even other planets and galaxies are being studied. These remote sensing methods are very suitable for studying and analysing more remote, inaccessible and vast areas. NASA (n.d.) has defined remote sensing as follows:

> Remote sensing is the acquiring of information from a distance. NASA observes Earth and other planetary bodies via remote sensors on satellites and aircraft that detect, and record reflected or emitted energy. Remote sensors, which provide a global perspective and a wealth of data about Earth systems, enable data-informed decision making based on the current and future state of our planet.

Sensors that use natural energy from the sun are called passive sensors; those that provide their own source of energy are called active sensors (Dyring 1973).

A vegetation index (VI) is computed using several spectral bands and a number that quantifies vegetation biomass or plant vigour for each pixel in space and aerial multispectral images (Geospatial Technology 2019). There are many different methods for analysing vegetation indices using spectral reflectance wavelengths obtained from passive remote sensing. Spectral reflectance wavelength has been identified as an effective method to sense and study vegetation and soil. Results from spectral reflectance measurements have been widely used in the agricultural sector, particularly to define land condition and the degree of land degradation, and to estimate AGB and crop yield (Scotford & Miller 2005). Measurement of the reflectance spectra of natural elements, such as vegetation, water, rock, and soil, allows researchers to gather information without requiring samples to be brought to the laboratory (Li et al. 2021). Various types of research and analysis have been carried out using vegetation indices (Musande et al. 2012).

The Sentinel-2 satellite, which is a widely used open source for remote sensing data, has sensors capable of recording reflectance spectra in the multi-channel spectral range (European Space Agency n.d.). Portable spectrometry equipment and multispectral drones can be used to obtain very high-resolution spectral reflectance data on plant condition and characteristics (Assmann et al. 2019). Connecting these data with satellite data from multispectral instruments, analysing and comparing them, and then machine-learning the classification, creates a wide range of possibilities (Bayaraa & Hirano 2015).

If AGB can be estimated with high accuracy, it will provide the basic data for determining the degradation of rangelands, as well as measures for restoration and sustainable use. The main goal of this study is therefore to combine remote sensing and field data with the overall aim to estimate AGB of rangelands in Mongolia.

Specific objectives:

1. To estimate AGB of the forest-steppe zone in Mongolia using the Random Forest (RF) modelling algorithm by integrating field sampling data with portable spectroradiometer, multispectral unmanned aerial vehicle (UAV), and Sentinel-2 Multispectral Instrument (MSI) datasets

2. To calculate vegetation indices based on the above mentioned three sets of remote sensing data and to choose the best correlations between vegetation biomass and vegetation indices.

2. MATERIALS AND METHODS

2.1 Study area

The study area is the entire forest-steppe zone of Mongolia which belongs to the main administrative unit of 11 provinces (Fig. 1). The total area of this natural zone is 221,000 km^2 or about 14.1% of the total area of Mongolia. About 143,000 km^2, or 64.7%, of the forest-steppe zone is rangeland. It accounts for about 13% of the total rangeland in Mongolia (ALAMGC 2020).

The study area is located between 46.42°-50.48° N, and 94.51°-113.15° E in the central-north of Mongolia. Semi-arid continental climate prevails in the area, and it has many high mountains and ridges, forests, and large lakes and ponds. Large rivers originate in, and flow through the region. The amount of precipitation varies due to different land elevations. In the period 1901-2021, the annual precipitation ranged from 336 to 482 mm and the average annual temperature ranged from -0.8°C to -5.6°C in 3 provinces (Arkhangai, Huvsgul, and Bulgan) of the forest-steppe zone (Climate Change Knowledge Portal 2021). The soil surface starts to freeze from mid-October and thaws in the first 10 days of April (Jambaajamts 1989).

2.2 Field sampling data

Field sampling was conducted in 69 field plots that fully represent the forest-steppe zone from 12th July to 8th August in 2021 and in 10 field plots from 24th to 31st July in 2022, during the peak plant growing season. All field plots were sampled according to monitoring plots of a NLMD [National land monitoring network database] at the ALAMGC [Agency for Land Administration and Management, Geodesy and Cartography]. When vegetation sampling was conducted in the field, measurements with the portable spectroradiometer were also taken and aerial images by multispectral UAV for the same periods were acquired.

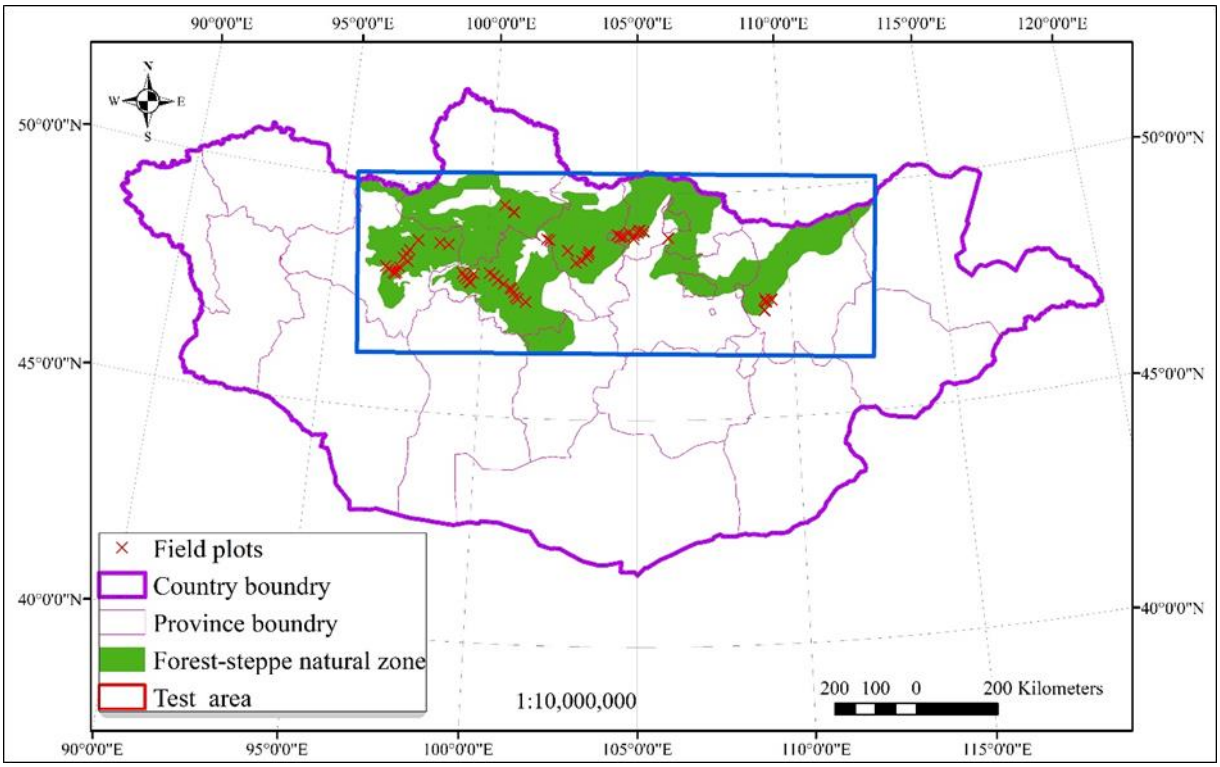

Figure 1. The forest-steppe zone in Mongolia and location of the field plots.

2.2.1 Field vegetation survey and vegetation biomass data

The dataset from 2021 includes data on the wet and dry weight of vegetation biomass and vegetation cover for all 69 sampling field plot (Appendix I). In addition, there is spectral reflectance data measured by the portable spectroradiometer for 39 of the plots (Appendix II). In July 2022, measurements were made at 10 sampling field plots. Of these, five plots coincide with sampling plots from 2021, while the remaining five plots were selected at unaffected locations that fully represent the vegetation and geography of the forest-steppe zone. For these 10 plots (Appendix III), aerial photographs were taken with a multispectral UAV, and measurements were taken with a portable spectroradiometer. Vegetation data was also collected.

After taking a reflectance spectrum measurement with the portable spectroradiometer and multispectral UAV, wet and dried AGB (gr / m^2), vegetation cover (%) (Wikum & Shanholtzer 1978), and vegetation height (cm) were measured for each plot according to a template as shown in Appendix IV, using a 0.5 m x 0.5 m frame (Fig. 2). The harvested grasses were cut at 1 cm above ground and the wet biomass was weighed. The harvested plants were dried at 80°C for 24 hours in the laboratory and then weighed for dried AGB.

a) b)

Figure 2. Vegetation survey in field plots: a) cutting wet biomass; b) vegetation cover measured using a 0.5 x 0.5 m frame. (Photos: M. Urtnasan, 30 July 2022).

2.2.2 Field spectrometry data and pre-processing

All vegetation reflectance spectra measurements were performed using an ASD FieldSpec 4 Standard-Res (Analytical Spectral Devices, Boulder, Colorado, USA) portable spectroradiometer between 11:00 am and 13:00 pm and only on sunny days without cloud cover. The vegetation reflectance spectra measurements were carried out using various spectroradiometer ranges and spectrum plates (Table 1).

Table 1. Specification of the ASD FieldSpec 4 Standard-Res portable spectroradiometer. (Source: From Malvern Panalytical a Spectris Company n.d).

No	Detectors	Spectral Resolution (nm)	Spectral sampling (bandwidth) (nm)	Spectral Range (nm)	Scanning Time (ms)
1	VNIR	3	1.4	350-1000	100
2	SWIR 1	10	1.1	1001-1800	
3	SWIR 2	10	1.1	1801-2500	

Generally, the portable spectroradiometer measurements were taken 1.6 m above the ground (Fig. 3) and recorded wavelengths between 350 and 2,500 nm (Table 1), which are the ranges of visible (Vis), short-wave infrared (SWIR), and near infrared (NIR) images used for identification of land surface elements. Reflectance spectra measurements were processed using ViewSpec Pro software. The data of the spectra measurements were further prepared for calculation of vegetation indices.

The vegetation indices of NDVI, DVI, MSAVI and EVI were calculated in Microsoft Excel 365 from the vegetation reflectance spectra measurements using values of the blue band at wavelength 490 nm, green band at wavelength 540 nm, red band at wavelength 665 nm, and NIR band at wavelength 842 nm.

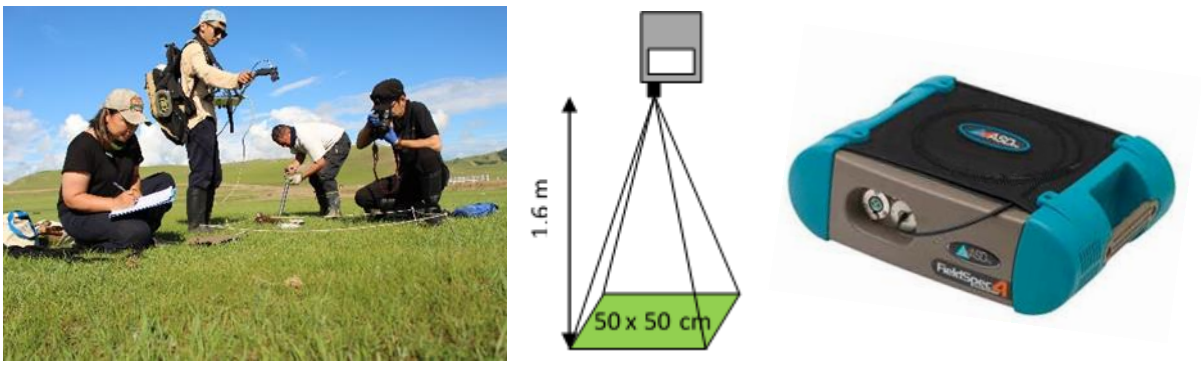

Figure 3. Portable spectroradiometer surveying in the field plots: left) capturing spectral measurements. (Photo: B. Batsaikhan, 30 July 2022); middle) portable spectroradiometer measurement scheme; right) ASD FieldSpec 4 Standard-Res portable spectroradiometer. (Source: From Malvern Panalytical a Spectris Company n.d.).

2.2.3 Multispectral UAV data and image pre-processing

Aerial multispectral images were obtained using a high precision multispectral UAV, the DJI Phantom 4 multispectral (P4M) drone. The P4M drone has five multispectral cameras with visible, blue, green, red, red edge, and NIR bands. Its spectrum range is 450-840 nm (Table 2).

Table 2. Band wavelengths of the DJI P4M drone cameras. (Source: From Dà-Jiang Innovations n.d.).

Band number	Description	Acronym	Central wavelength (nm)	Wavelength width (nm)
1	Blue	B	450 ±16	32
2	Green	G	560 ±16	32
3	Red	R	650 ±16	32
4	Red Edge	RE	730 ±16	32
5	Near-Infrared	NIR	840 ±16	52

The aerial multispectral images were taken between 11:00 am and 13:00 pm, on sunny and cloud-free days only, and captured an area of 100 x 100 m at 60 meters above ground. The focal length of the DJI P4M drone camera was 4.5 mm. The duration of flight missions was around 15 minutes for each field plot, covering the entire plot with an overlap of 80% between images and 70% between lines. The aerial multispectral images were processed using Agisoft software. RGB and NDVI raster images for sampling field number 8, built on the DJI P4M drone dataset, are shown in Figure 4.

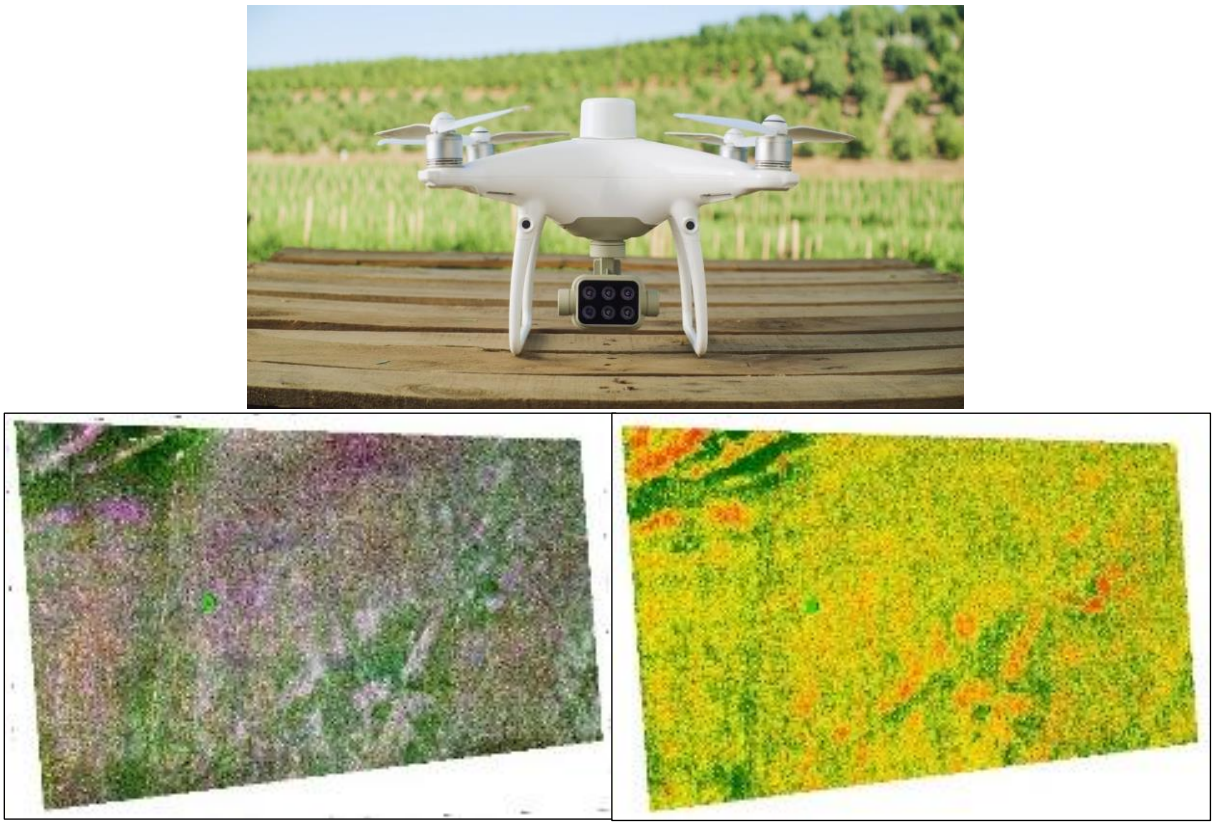

Figure 4. Multispectral aerial images and multispectral UAV used for aerial image acquisition: top) DJI P4M drone; bottom left) true colour RGB raster image, including all five bands; bottom right) NDVI raster image calculated using band 3 and band 5.

The Raster Calculator tool of QGIS 3.26.2 software was used to calculate NDVI, DVI, MSAVI and EVI using the DJI P4M drone datasets. When extracting point values of vegetation indices, the Zonal Statistic as Table tool of ArcMAP 10.8.1 was used; extracted values are the mean value of a circle with a 0.5 m diameter.

2.3 Sentinel-2 Multispectral Instrument dataset and pre-processing

The purpose of the Sentinel-2 satellite is to provide remote sensing data for land use, land cover and disaster monitoring (Phiri et al. 2020). Sentinel-2 MSI images are open access and offer higher spatial resolution and quicker temporal resolution than other satellites, such as MODIS [The Moderate Resolution Imaging Spectroradiometer] and Landsat series satellites. The Sentinel-2 MSI datasets are used for regional monitoring of land use and land cover, and for studies of land surface conditions and changes. The Sentinel-2 MSI consists of two sensors: Sentinel-2A, launched in 2015, and Sentinel-2 launched in 2017. The Sentinel-2 MSI measures the Earth's reflected radiance on 13 spectral bands and has high spatial-temporal resolution. The pixel size is 10-60 m and the revisit time is five days. The spectrum range is 442-2202 nm, as detailed in Table 3 (Europian Space Agency n.d.)

Table 3. Spectral bands of the Sentinel-2 MSI. (Source: From European Space Agency n.d.).

Band number	Description	S2A		S2B		Spatial resolution (m)
		Central wavelength (nm)	Bandwidth (nm)	Central wavelength (nm)	Bandwidth (nm)	
1	Ultra-blue	442.7	20	442.3	20	60
2	Red	492.7	65	492.3	65	10
3	Green	559.8	35	558.9	35	10
4	Blue	664.6	30	664.9	31	10
5	VNIR	704.1	14	703.8	15	20
6	VNIR	740.5	14	739.1	13	20
7	VNIR	782.8	19	779.7	19	20
8	VNIR	832.8	105	832.9	104	10
8a	VNIR	864.7	21	864.0	21	20
9	SWIR	945.1	19	943.2	20	60
10	SWIR	1373.5	29	1376.9	29	60
11	SWIR	1613.7	90	1610.4	94	20
12	SWIR	2202.4	174	2185.7	184	20

Sentinel-2 MSI datasets were obtained using JavaScript in the Google Earth Engine (GEE) computing platform. The NIR (B08), red (B04), and blue (B02) bands were used for this study. Raster images were mapped from the Sentinel-2 MSI dataset, when cloud cover was 15% or less. The obtained Sentinel-2 MSI datasets were from dates coinciding with the field sampling, or from 12 July to 8 August in 2021 and from between 24 and 31 July in 2022. Raster images of NVDI, DVI, MSAVI and EVI from GEE were exported to google drive storage and then downloaded to my laptop hard drive. To extract point values of vegetation indices, the Zonal Statistic as Table tool of ArcMAP 10.8.1 was used. Mean values from 10 x 10 m pixel raster images of vegetation indices were extracted using the Sentinel-2 MSI datasets.

2.4 Vegetation indices

In this study, four vegetation indices were utilized: NDVI, DVI, MSAVI, and EVI (Fig. 5 and 6). They were calculated according to the formulas shown in Table 4 and processed using the GEE computing platform. The dates were the same as for field sampling.

Table 4. Formulas for calculation the spectral vegetation indices.

Vegetation index	Acronym	Equation	References
Normalized Difference Vegetation Index	NDVI	$(P_{NIR} - P_{Red}) / (P_{NIR} + P_{Red})$	(Rouse et al. 1973)
Difference Vegetation Index	DVI	$(P_{NIR} - P_{Red})$	(Tucker 1979)
Modified Soil Adjusted Vegetation Index	MSAVI	$(2 \times P_{NIR} + 1 - \text{sqrt} ((2 \times P_{NIR} + 1)^2 - 8 \times (P_{NIR} - P_{Red}))) / 2$	(Qi et al. 1994)
Enhanced Vegetation Index	EVI	$2.5 \times (P_{NIR} - P_{Red}) / (P_{NIR} + 6 \times P_{Red} - 7.5 \times P_{Blue} + 1)$	(Liu & Huete 1995)

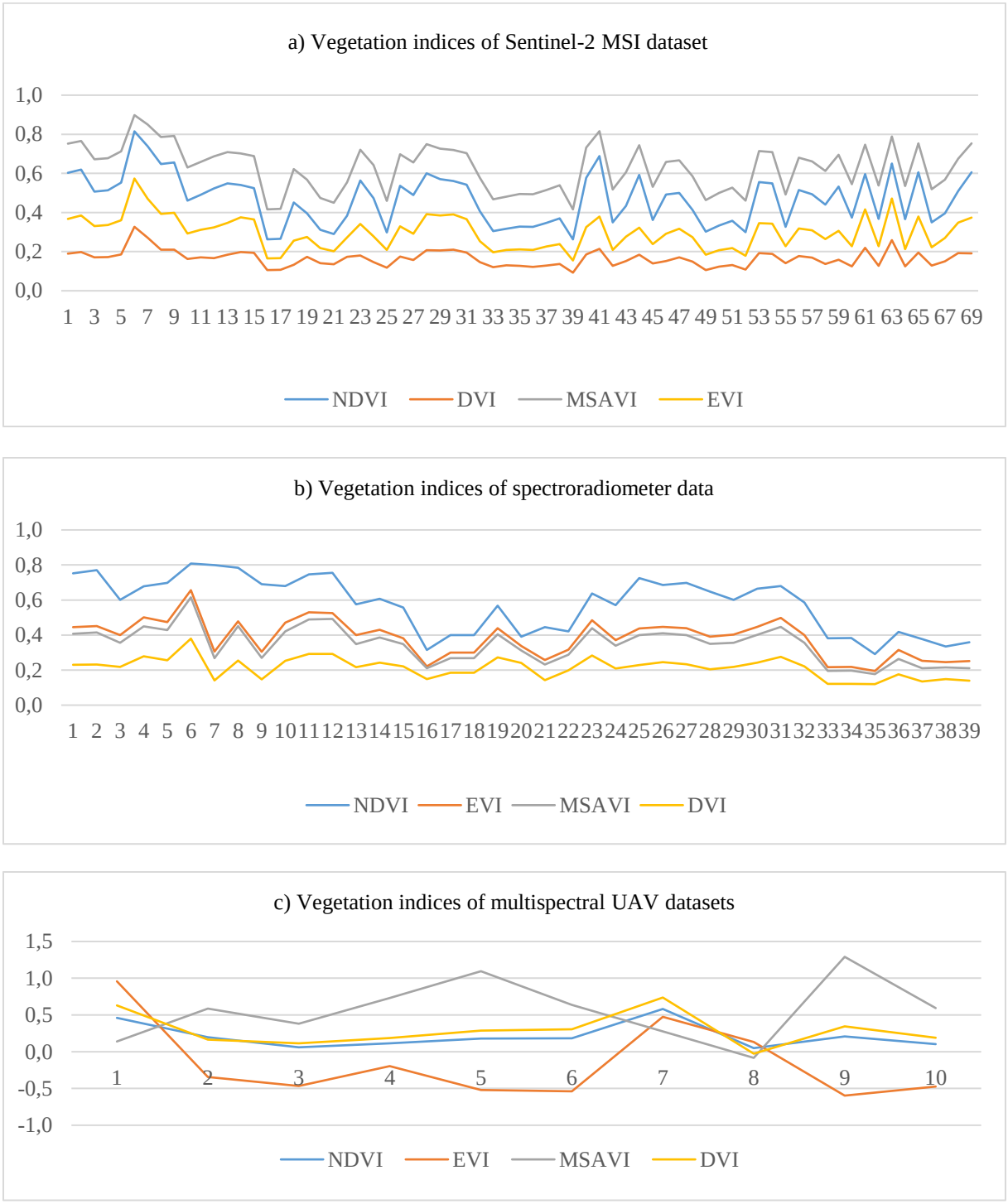

Figure 5. Comparison of vegetation indices calculated from different sources: a) vegetation indices calculated from the Sentinel-2 MSI dataset; b) vegetation indices calculated from the portable spectroradiometer data; c) vegetation indices calculated from DJI P4M drone datasets.

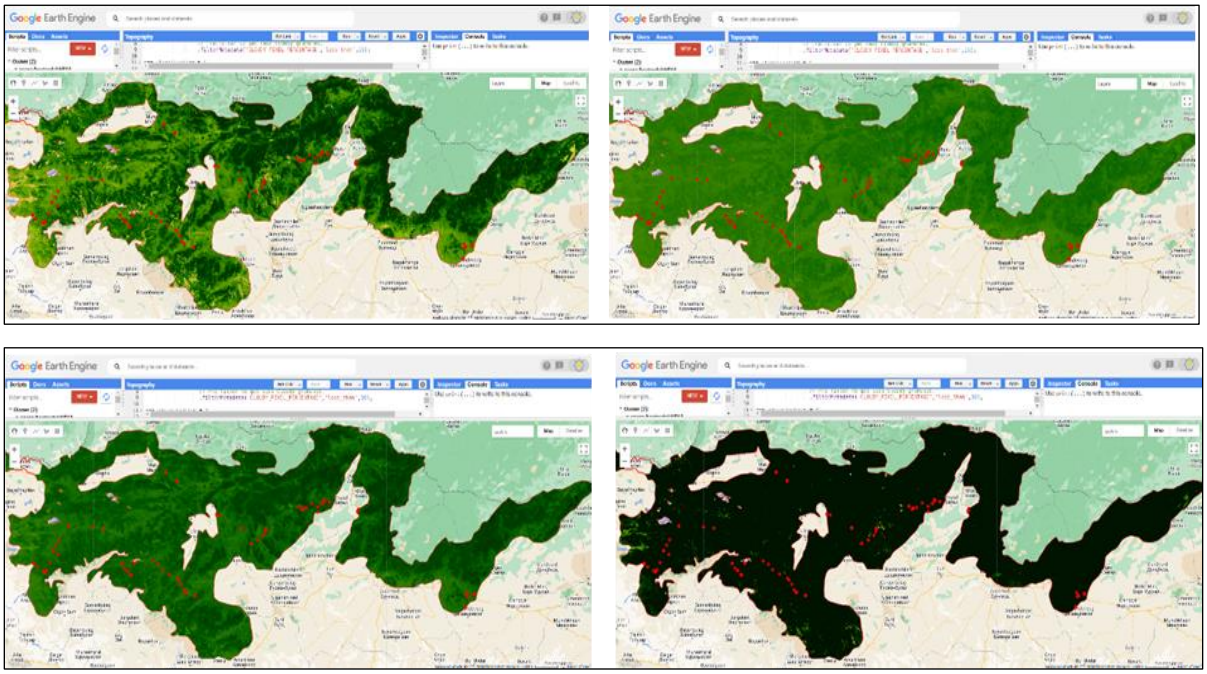

Figure 6. Raster images of vegetation indices for the study area in July and August of 2021, calculated using JavaScript in the GEE computing platform: top left) NDVI raster image; top right) DVI raster image; bottom left) EVI raster image; bottom right) MSAVI raster image.

2.5 Workflow

The workflow for the whole process of using remote sensing datasets and vegetation sampling to develop a model estimation AGB in the forest-steppe zone in Mongolia is shown in Fig. 7.

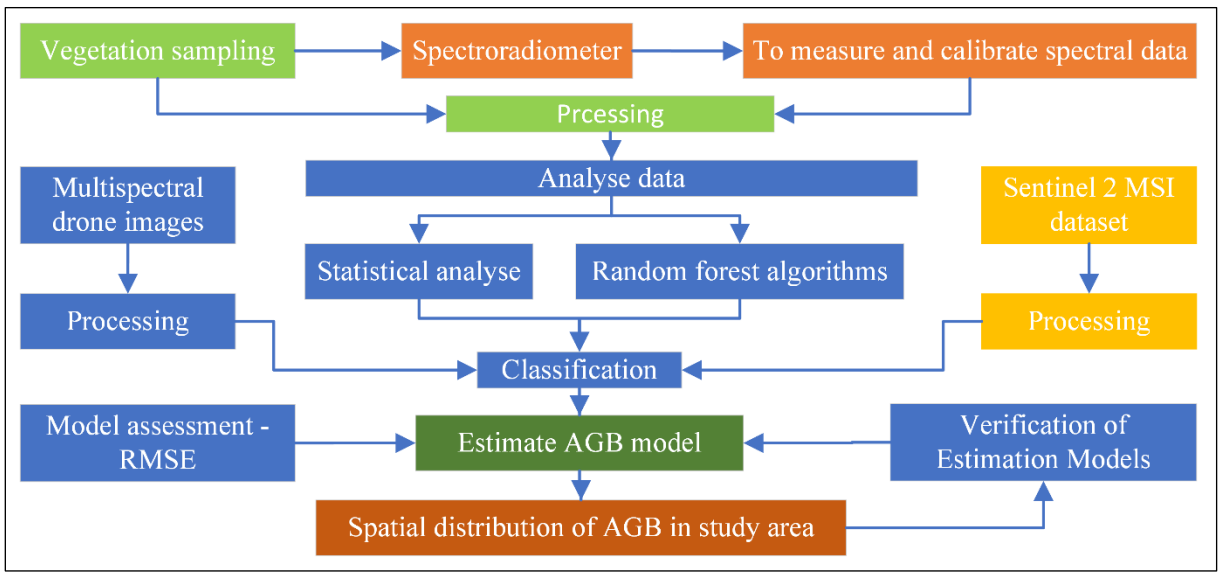

Figure 7. Methodology and work flow for model estimation of above ground biomass (AGB) using vegetation sampling and remote sensing data, such as portable spectroradiometer, DJI P4M drone, and Sentinel-2 MSI datasets.

2.6 Statistical analysis

The statistical analyses were carried out in Python 3.11 using Jupiter Notebook (Anaconda 3) and Microsoft Excel 365. The relationship between vegetation indices and vegetation wet biomass and vegetation dried biomass during the growth peak period were analysed using sampling field plot data.

A linear regression statistical analysis was used to test if vegetation indices significantly predicted wet and dry biomass. Linear regression was carried out between vegetation wet biomass, dried biomass and four vegetation indices which were calculated from the portable spectroradiometer, DJI P4M drone and Sentinel-2 MSI datasets, using the Python scripts in Jupiter Notebook software.

2.7 Algorithms for modelling AGB

The RF is an algorithm that was developed by Beiman (Li et al. 2021) and is one of the tree-based models. The RF algorithm is supervised machine learning that is used for data analysis (Ho 1995) and it is now widely used for a variety of applications, such as biomass estimation and raster image classification (Erdenebaatar et al. 2021). RF works on randomly selected data samples to create a decision tree and assessment classification (Jin et al. 2020). The algorithm works according to the following four steps: a) select random samples from a dataset; b) construct a decision tree and get prediction results; c) vote among predicted results; d) perform a final prediction (Ho 1995).

The RF model with a combination variable of raw bands and NDVI and MSAVI vegetation indices derived from Sentinel-2 MSI and portable spectroradiometer was implemented in this project using the Scikit-learn package in Python 3.11.

2.8 Model assessment

Root mean square error (RMSE) is one of the most common measures to estimate the accuracy of forecasting models. It compares predicted versus observed values while training the regression models (Willmott & Matsuura 2005). RMSE is estimated according to Equation 1,

$$RMSE = \sqrt{\sum_{i=1}^{n} \frac{(\hat{y}_i - y_i)^2}{n}} \qquad (1)$$

where y_i represents the field measured and $\hat{y}_i$ represents estimated AGB values, and n represents the size of the samples in dataset.

RF model estimation of AGB investigates the application of remote sensing-based vegetation indices, performing a classification for estimating AGB. The relationship between the wet and dry biomass sampling data and the vegetation indices derived from Sentinel-2 MSI (Erdenebaatar et al. 2021) and portable spectroradiometer results performed relatively well in predicting the AGB.

3. RESULTS

3.1 Relationship between biomass and vegetation indices

A total number of 42 regression models were estimated in this study. The top ten correlation results were selected from these regression models to develop the RF model estimation of AGB (Figure 8-11).

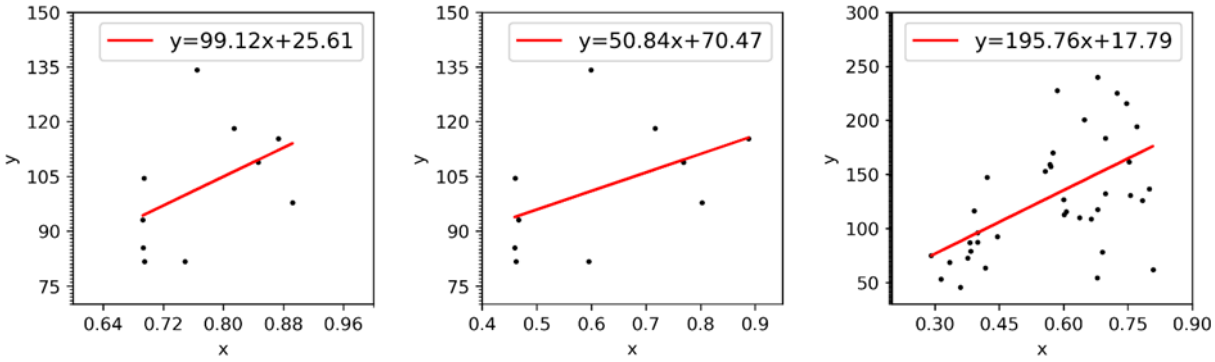

Figure 8. Relationship between dried biomass and, left) the NDVI of the portable spectroradiometer in 2022; middle) the EVI of the portable spectroradiometer in 2021; and right) relationship between wet biomass and NDVI of the portable spectroradiometer in 2021.

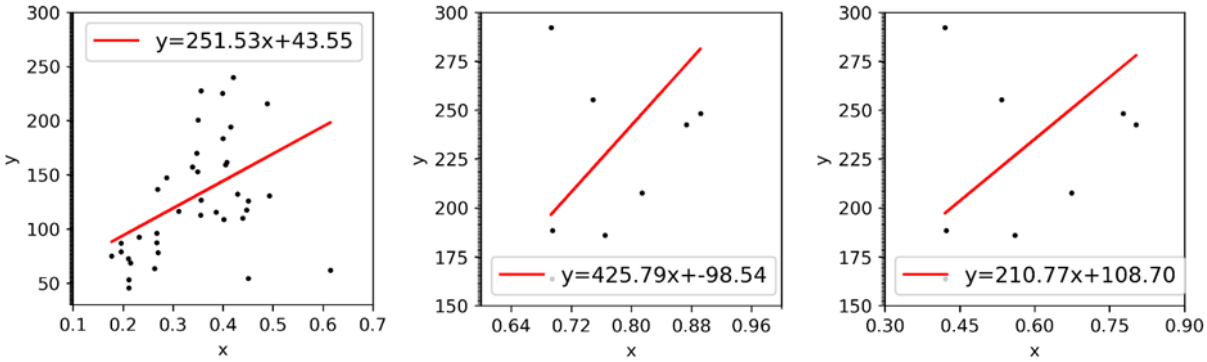

Figure 9. Relationship between wet biomass and left) the MSAVI of the portable spectroradiometer in 2021; middle) the NDVI of the portable spectroradiometer in 2022; and right) the MSAVI of the portable spectroradiometer in 2022.

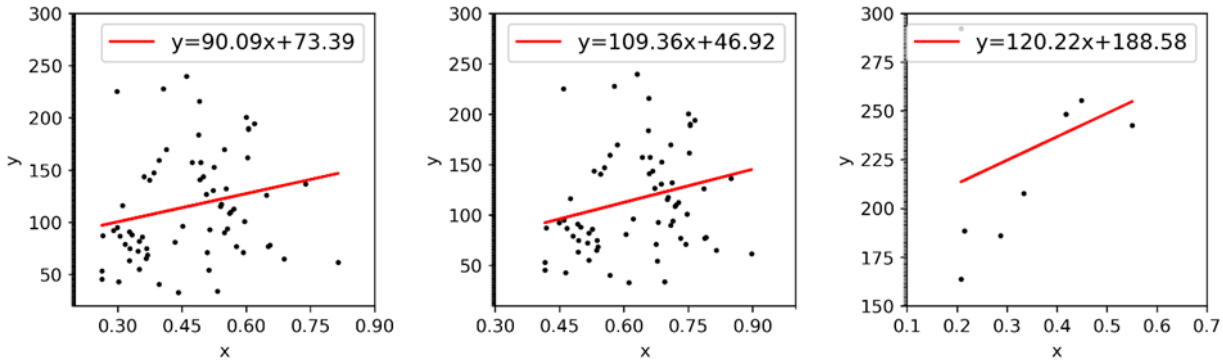

Figure 10. Relationship between wet biomass and left) the NDVI of the Sentinel-2 MSI in 2021; middle) the MSAVI of the Sentinel-2 MSI in 2021; and right) the NDVI of the Sentinel-2 MSI in 2022.

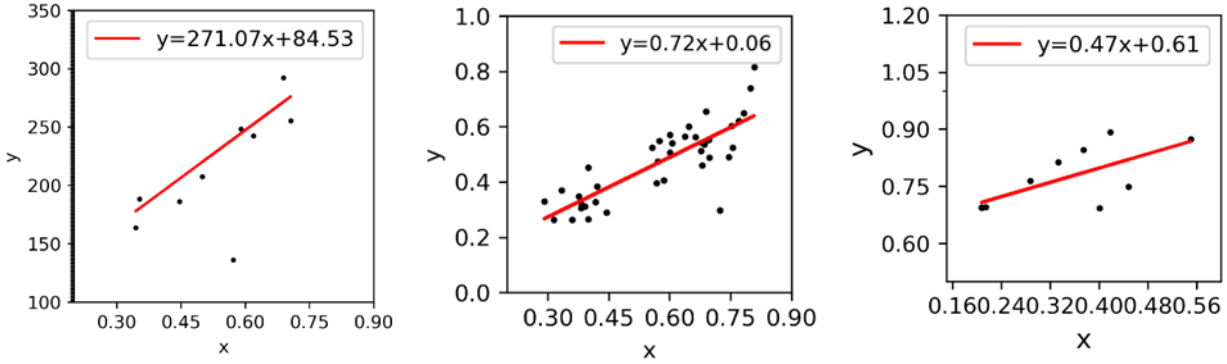

Figure 11. Left) Relationship between wet biomass and the MSAVI of the Sentinel-2 MSI in 2022; middle) relationship between NDVI of the Sentinel-2 MSI and NDVI of the portable spectroradiometer in 2021; and right) relationship between NDVI of the Sentinel-2 MSI and NDVI of the portable spectroradiometer in 2022.

The analysis of the relationship between the dried biomass and the vegetation indices showed a correlation in the range from -0.0705 to 0.4736 (Table 5). The correlation between the wet biomass and vegetation indices was from -0.001 to 0.5068 (Table 6). Most of the relationships between vegetation indices from the DJI P4M drone dataset and the vegetation biomass were negatively correlated as shown in Table 5 and 6. Therefore, it was considered unnecessary to use the DJI P4M drone dataset and vegetation indices derived from the DJI P4M drone in this study.

The selected regression models with the best correlation for use to develop the model estimation of AGB are marked with an asterisk (*) in Tables 5 and 6. The results are as follows: 1) the correlation between dried biomass and NDVI of the portable spectroradiometer in 2022 is 0.4526, 2) the correlation between dried biomass and EVI of the portable spectroradiometer in 2022 is 0.4736 (Table 5), 3) the correlation between wet biomass and NDVI of the portable spectroradiometer in 2021 is 0.5068, 4) the correlation between wet biomass and MSAVI of the portable spectroradiometer in 2021 is 0.4193, 5) the correlation between wet biomass and NDVI of the portable spectroradiometer in 2022 is 0.4803, 6) the correlation between wet biomass and MSAVI of the portable spectroradiometer in 2022 is 0.4644, 7) the correlation between wet biomass and NDVI of the Sentinel-2 MSI in 2021 is 0.4036, 8) the correlation

between wet biomass and MSAVI of the Sentinel-2 MSI in 2021 is 0.3292, 9) the correlation between wet biomass and NDVI of the Sentinel-2 MSI in 2022 is 0.4179, 10) the correlation between wet biomass and MSAVI of the Sentinel-2 MSI in 2022 is 0.4849 (Table 6).

Based on the correlation, I decided to use NDVI and MSAVI calculated from the Sentinel-2 MSI dataset and NDVI calculated from the portable spectroradiometer data to develop the RF model estimation of AGB. Moreover, the following Sentinel-2 MSI spectral bands were used to develop the RF model estimation of AGB: band 2 (blue), band 3 (green), band 4 (red) and band 8 (NIR).

Table 5. Relationship between dried biomass and vegetation indices (2021-2022), where *db* represents vegetation dried biomass and *y* represents related vegetation indices in the regression model formula.

Vegetation indices	Regression model	Correlation	R^2
Vegetation indices of portable spectroradiometer (2021)			
NDVI		0.1998	0.0399
EVI		0.1841	0.0339
MSAVI		0.1921	0.0369
DVI		0.1752	0.0307
Vegetation indices of portable spectroradiometer (2022)			
NDVI	$y = 99.12 \times db + 25.61$	0.4526*	0.2048
EVI	$y = 50.84 \times db + 70.47$	0.4736*	0.2243
MSAVI		0.3808	0.1450
DVI		0.2933	0.0860
Vegetation indices of multispectral UAV (2022)			
NDVI		-0.0705	0.0050
EVI		-0.2630	0.0692
MSAVI		0.3249	0.1056
DVI		0.4119	0.1697
Vegetation indices of Sentinel-2 MSI (2021)			
NDVI		0.147	0.0217
EVI		0.026	0.0007
MSAVI		0.0402	0.0016
DVI		0.044	0.0019
Vegetation indices of Sentinel-2 MSI (2022)			
NDVI		0.14	0.0196
EVI		0.1967	0.0387
MSAVI		0.1309	0.0171
DVI		0.293	0.0858

Table 6. Relationship between vegetation wet biomass and vegetation indices (2021-2022), where *wb* represents vegetation wet biomass and *y* represents related vegetation indices in the regression model formula.

Vegetation indices	Regression model	Correlation	R^2
Vegetation indices of portable spectroradiometer (2021)			
NDVI	y = 195.76 × wb + 17.79	0.5068*	0.2568
EVI		0.4189	0.1755
MSAVI	y = 251.53 × wb + 43.55	0.4193*	0.1758
DVI		0.3469	0.1203
Vegetation indices of portable spectroradiometer (2022)			
NDVI	y = 425.79 × wb + -98.54	0.4803*	0.2307
EVI		0.4716	0.2224
MSAVI	y = 210.77 × wb + 108.7	0.4644*	0.2157
DVI		0.4422	0.1955
Vegetation indices of multispectral UAV (2022)			
NDVI		-0.2747	0.0755
EVI		-0.0928	0.0086
MSAVI		-0.0010	0.0000
DVI		-0.1270	0.0161
Vegetation indices of Sentinel-2 MSI (2021)			
NDVI	y = 90.09 × wb + 73.39	0.4036*	0.1629
EVI		0.1648	0.0272
MSAVI	y = 109.36 × wb + 46.92	0.3292*	0.1084
DVI		0.2096	0.044
Vegetation indices of Sentinel-2 MSI (2022)			
NDVI	y = 120.22 × wb + 188.58	0.4179*	0.3113
EVI		0.3326	0.1106
MSAVI	y = 271.07 × wb + 84.53	0.4849*	0.2351
DVI		0.3849	0.1482

Three kinds of NDVI calculated from different datasets were compared and analysed. When analysing the data collected in 2022, the NDVI calculated from the DJI P4M drone had a slightly negative correlation with the NDVI calculated from the Sentinel-2 MSI and the portable spectroradiometer (Table 7). But when comparing the NDVI calculated from the Sentinel-2 MSI and the NDVI calculated from the portable spectroradiometer, there was a high correlation for both years (Table 8).

Table 7. Relationship between NDVI calculated from different datasets in 2022, where $NDVI_{DRO}$ represents NDVI of DJI P4M drone, $NDVI_{SEN}$ represents NDVI of Sentinel-2 and $NDVI_{SRM}$ represents NDVI of the portable spectroradiometer in regression model formula.

Relationship	NDVI of Sentinel-2 MSI (2022)			NDVI of portable spectroradiometer (2022)		
	Regression model	**Correlation**	**R^2**	**Regression model**	**Correlation**	**R^2**
NDVI of DJI P4M drone (2022)	$NDVI_{DRO} = - 0.55 \times NDVI_{SEN} + 0.4$	- 0.3632	0.132	$NDVI_{DRO} = - 0.04 \times NDVI_{SRM} + 0.78$	- 0.092	0.009

Table 8. Relationship between NDVI calculated from different datasets in 2021-2022, where $NDVI_{SEN}$ represents NDVI of Sentinel-2 and $NDVI_{SRM}$ represents NDVI of portable spectroradiometer in regression model formula.

Relationship	NDVI of portable spectroradiometer (2021)			NDVI of portable spectroradiometer (2022)		
	Regression model	**Correlation**	**R^2**	**Regression model**	**Correlation**	**R^2**
NDVI of Sentinel-2 MSI (2021)	$NDVI_{SEN} = 0.72 \times NDVI_{SRM} + 0.06$	0.8165	0.667	-	-	-
NDVI of Sentinel-2 MSI (2022)	-	-	-	$NDVI_{SEN} = 0.47 \times NDVI_{SRM} + 0.61$	0.6802	0.463

3.2 Development and validation of estimation models

In this study, I selected the highest correlation combination variable with vegetation wet biomass and NDVI and MSAVI calculated from the Sentinel-2 MSI dataset and NDVI calculated from the portable spectroradiometer data, and band 8 (NIR), band 4 (Red), band 3 (Green), and band 2 (Blue) of the Sentinel-2 MSI. RF model estimation of AGB was estimated using the Scikit-learn package in Jupiter Notebook (Anaconda 3) software.

The RF model estimation of AGB randomly utilized 20% of the sampling data for testing the algorithm and 80% for training the algorithm. The results are shown in Figure 12 (a). Results of verification and assessment RF model are shown in Figure 12 (b, c) and Table 9.

a)

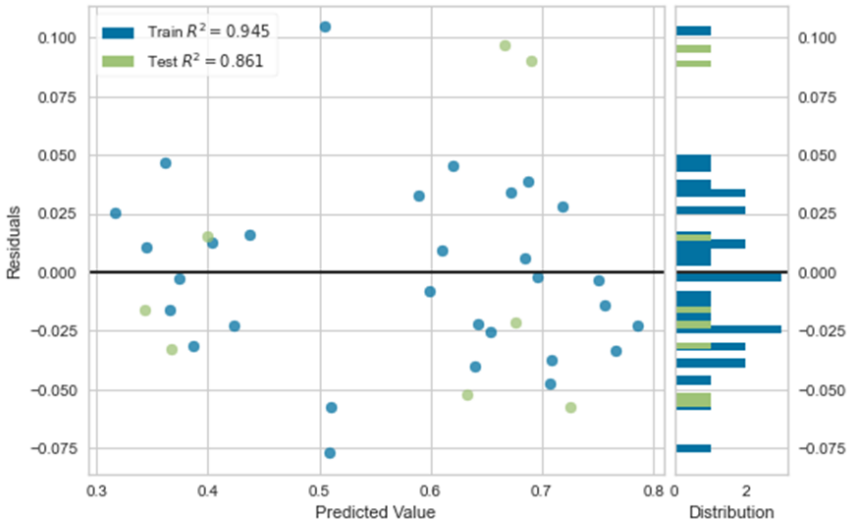

b)

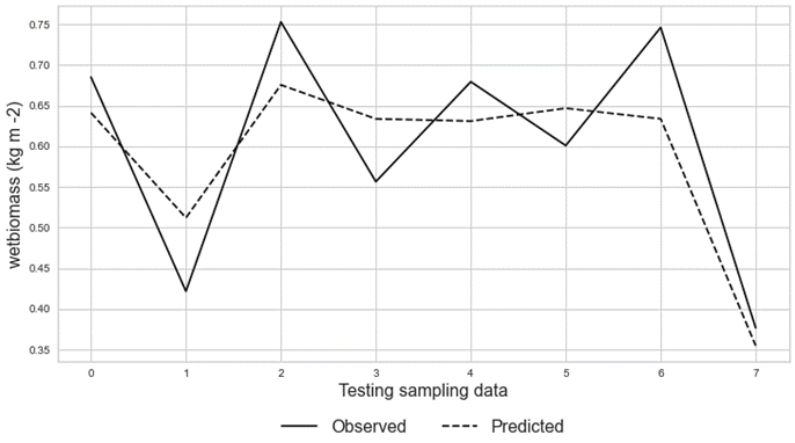

c)

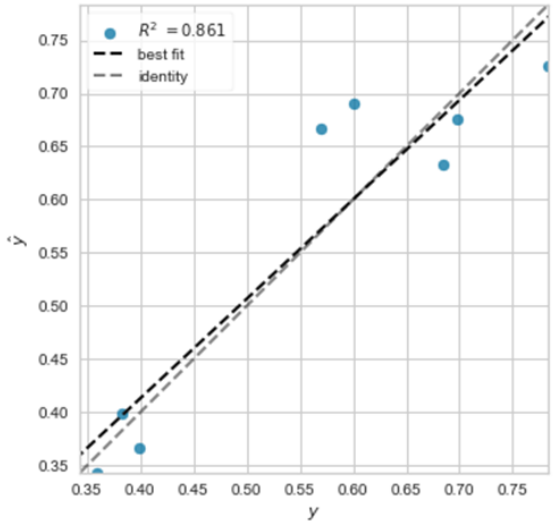

Figure 12. Comparing predicted and observed values of AGB using the RF model: a) residuals for RF model estimation of AGB; b) comparison between observed AGB of the sampling data and predicted AGB of testing sampling data; c) prediction error for the RF model estimation of AGB.

Table 9. RMSE of RF model estimation of AGB.

Model	RF model		
	RMSE kg/ha	R^2	RMSE %
Raw bands, vegetation indices	36.3	0.94	0.165

3.3 Spatial distribution of biomass in the forest-steppe of Mongolia

To minimise time for processing and downloading from the GEE computing platform, a smaller test area than the study area was chosen for spatial distribution mapping. The area is about 10,000 ha. The estimated AGB using the RF model for each pixel of the selected area and the AGB spatial distribution map are shown in Figure 13.

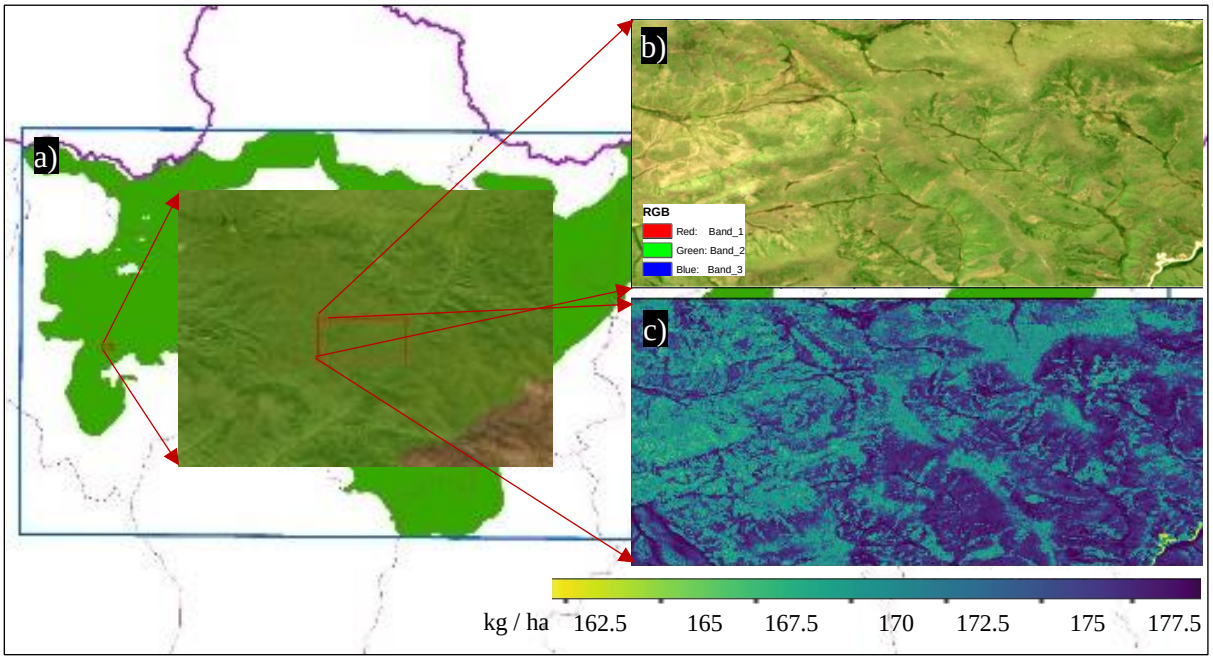

Figure 13. Sample predicted AGB raster images using the RF model for the test area: a) location of the test area, b) natural colour raster images of Sentinel-2 MSI, c) Raster image of the predicted AGB.

4. DISCUSSION

Because there exist so many vegetation indices derived from spectral measurement of optical sensors, it was important to find the most appropriate vegetation indices for estimating AGB in the forest-steppe zone of Mongolian rangelands. This is because the spectral reflectance characteristics of plants are related to vegetation biomass, soil moisture, species, and plant growth stage (Roy 1989). Jin et al. 2014 studied NDVI and their approach is widely used for estimating AGB, while MSAVI is used for estimating AGB of rangeland with low vegetation cover. Some related studies have had varying success using optical sensors with different spatial and spectral resolutions to estimate AGB, though the accuracy of these models has been limited (Lu 2006). In this study, NDVI and MSAVI were used to develop the RF model estimation of AGB and the results met the objectives of the study. Therefore, the developed RF model for

estimation of AGB can be introduced in Mongolia, and the machine learning algorithm can be enriched with more sample data to further improve it.

Jin et al. (2014) calculated the correlation between NDVI, DVI, MSAVI and other vegetation indices derived from a MODIS dataset. Their correlations were 0.6-0.7 for Xilingol, Inner Mongolia in Northern China. In this study, the correlation was lower at 0.3293-0.5068 (Tables 5 and 6).

Noteworthy results from this study are that correlation between vegetation indices derived from the DJI P4M drone dataset and vegetation biomass was mostly negative. The NDVI derived from the DJI P4M drone was also negatively related to the NDVI derived from the Sentinel-2 MSI and portable spectroradiometer. These results did not meet expectations. Although the DJI P4M drone has a very high resolution, there is a need to investigate the reason for the negative correlation with vegetation biomass and NDVI derived from other sources. The reason for this is likely to be that the area used to extract the mean value of wavelengths from DJI P4M drone bands was the same as the area measured by the portable spectroradiometer, i.e. 0.5 x 0.5 m. It might be a good idea to enlarge the size of this area and to extract the mean value of wavelengths from a larger area in a future study.

The result of the analysis using the DJI P4M drone dataset from 2022 was unsatisfactory. Further research is needed to develop RF model estimation of AGB using multispectral UAV datasets such as aerial multispectral raster images acquired by DJI P4M drones.

The evaluated precision of the RF model estimation of AGB was good as shown in Table 9 and Figure 12. Furthermore, the results of the predicted AGB using the RF model, shown in Table 9, indicate a good fit using RF algorithm modelling accuracy to estimate AGB in the forest-steppe. In "The methods of monitoring rangeland using remote sensing" from ALAMGC, modelling accuracy of this method was said to be $R^2 = 0.95$.

5. CONCLUSIONS

This study used an RF machine learning algorithm with multispectral bands (NIR, red, green and blue), vegetation indices (NDVI, DVI, MSAVI and EVI) derived from Sentinel-2 MSI, DJI P4M drone and a portable spectroradiometer, and vegetation biomass collected from field plots. Above ground biomass (AGB) was estimated using the developed RF model in a test area and the predicted and observed values of AGB were then compared with sampling data. The results showed that vegetation indices and spectral bands derived from the Sentinel-2 MSI and the portable spectroradiometer have good potential in RF model estimation of AGB in the forest-steppe zone of Mongolian rangelands.

In this study, it was ensured that the timing of the field plot sampling and the acquisition dates for the remote sensing data coincided as much as possible. This approach is believed to have improved the sensitivity of the remote sensing dataset to reflect AGB in rangeland. This is because remote sensed spectral values can change depending on weather conditions. Therefore, it is important that remote sensing data received from different sources are close in time.

Because the machine learning algorithm was used to develop the model estimation AGB, the more sampling data with spectral measurements can be added and the modelling accuracy can be further improved.

The developed model estimation of AGB can save manpower, time and reduce costs for rangeland monitoring in the forest-steppe zone of Mongolia. Using the basic methodology of the developed RF model estimation of AGB, it is quite possible to develop and introduce estimation AGB modelling in other natural zones in Mongolia, such as steppe, desert steppe (Gobi), and desert.

ACKNOWLEDGEMENTS

I would like to thank all the staff of the GRÓ LRT Land Restoration Training Programme, under the auspices of UNESCO, for giving me this great opportunity. I am most grateful to director Sjöfn Vilhelmsdóttir, deputy programme director Berglind Orradóttir, office manager Halldóra Traustadóttir, and Brita Berglund for their generous support, clear guidance, and assistance for the entire programme.

I would like to express gratitude to my supervisor, Asra Salimi, and to the project coordinator, Berglind Orradóttir, for their clear guidance and contribution to my successful completion of this research project. With their support and assistance, I learnt new analysis in my research field and improved my academic writing skills a lot.

Moreover, I would like to thank all the lecturers who shared their knowledge and experiences during the training. All the lectures improved my knowledge and broadened my horizon about land degradation and restoration.

I sincerely thank my beloved family: my father Baatar Samdanmunkh and my mother Erdenesuvd Nyamsuren, my wife Oyuntuya Purevdorj, my son Suld D and my daughter Bayasgalan D. Thanks to my friends for help and support.

I also greatly appreciate the support of my colleagues Ankhbayar G and Enkhjargal N at the Division of Land Monitoring, Agency for Land Administration and Management, Geodesy and Cartography, and Urtnasan M at the Division of Remote Sensing and Spatial Modelling, Institution of Geography and Geo-Ecology for assistance in the field data collection.

Finally, I thank all the GRÓ LRT fellows from 2022 who made my stay in Iceland very memorable.

LITERATURE CITED

ALAMGC (2020) The unified land territory 2020 report. Munkhiin-Useg printing, Ulaanbaatar.

Assmann JJ, Kerby JT, Cunliffe AM, Myers-Smith IH (2019) Vegetation monitoring using multispectral sensors - best practices and lessons learned from high latitudes. Journal of Unmanned Vehicle Systems 7:54-75

Bayaraa B, Hirano A (2015) Mapping summertime pasture amount in north central. Pages 1060-1065. In: Asian Conference on Remote Sensing. ACRS 2012: Proceedings of 33rd Asian Conference on Remote Sensing, Pattaya, Thailand, 26-30 November 2012. Curran Associates, New York

Climate Change Knowledge Portal (2021) Climatology. https://climateknowledgeportal.worldbank.org/country/mongolia/climate-data-historical#:~:text=Average%20temperatures%20range%20between%20around,varies%20dramatically%20throughout%20the%20year (accessed 01 Sep 2022)

Dà-Jiang Innovations (n.d) P4 Multispectral. https://www.dji.com/p4-multispectral?site=brandsite&from=nav (accessed 30 July 2022)

Dagvadorj D, Tennigkeit T, Wilkes A, Yeager C (2013) Nationally appropriate mitigation actions for grassland and livestock management in Mongolia. Asian Development Bank. https://www.adb.org/sites/default/files/publication/30256/nationally-appropriate-mitigation-actions-mongolia.pdf

Densambuu B, Indree T, Battur A, Sainnemekh S (2018a) State and transition model of rangeland. Second edition. Sod press publisher, Ulaanbaatar

Densambuu B, Sainnemekh S, Bestelmeyer B, Ulambayar B (2018b) National report of the rangeland condition of Mongolia. Selenge press, Ulaanbaatar

Dorj M, Ulambayar B, Densambuu B (2021) Бэлчээр ашиглалтын нөлөөг хянах фото мониторингийн үндэсний тайлан [National report of the Grazing impact monitoring of Mongolia]. Sod press publisher, Ulaanbaatar (in Mongolian)

Dyring E (1973) Principles of remote sensing. Ambio 11:57-69

Erdenebaatar N, Bayaraa B, Damdinsuren A (2021) Application of random forest approach to biomass estimation using remotely sensed data. Advances in Engineering Research 206:109-115

European Geosciences Union (2014) Article. https://gmd.copernicus.org/articles/7/1247/2014/gmd-7-1247-2014.html (accessed 10 June 2022)

European Space Agency (n.d.) Multispectral instrument overview. https://sentinels.copernicus.eu/web/sentinel/technical-guides/sentinel-2-msi/msi-instrument (accessed 13 July 2022)

Geospatial Technology (2019) What does vegetation index mean in remote sensing technology? https://mapasyst.extension.org/what-does-vegetation-index-mean-in-remote-sensing-technology/ (accessed 22 July 2022)

Godde CM, Boone RB, Ash AJ, Waha K, Sloat LL, Thornton PK, et al. (2020) Global rangeland production systems and livelihoods at threat under climate change and variability. Environmental Research Letters 15:1-15

Humboldt State University (n.d.) History of remote sensing. http://gsp.humboldt.edu/olm/Courses/GSP_216/online/lesson1/history.html (accessed 10 July 2022)

Ho TK (1995) Random decision forests. Proceedings of the International Conference on Document Analysis and Recognition 1:278-282

ILRI (International Livestock Research Institute), IUCN, FAO, WWF, UNEP (2021) Rangelands atlas. ILRI, Nairobi Kenya

Jigjidsuren S, Johnson DA (2003) Forage plants of Mongolia. Admon, Ulaanbaatar

Jin Y, Yang X, Qiu J, Li J, Gao T, Wu Q, et al. (2014) Remote sensing-based biomass estimation and its spatio-temporal variations in temperate grassland, Northern China. Remote Sensing 6:1496-1513

Jin Z, Shang J, Zhu Q, Ling C, Xie W, Qiang B (2020) RFRSF: Employee turnover prediction based on random forests and survival analysis. Pages 503-515. In: Web information systems engineering – WISE 2020: Proceedings of the 21st International Conference, Amsterdam, The Netherlands, October 20-24, 2020. Springer, Berlin

Li C, Zhou L, Xu W (2021) Estimating aboveground biomass using Sentinel-2 MSI data and ensemble algorithms for grassland in the Shengjin lake wetland, China. Remote Sensing 13:1-18

Liu HQ, Huete A (1995) A feedback-based modification of the NDVI to minimize canopy background and atmospheric noise. IEEE Transactions on Geoscience and Remote Sensing 33:457-465

Lu D (2006) The potential and challenge of remote sensing-based biomass estimation. International Journal of Remote Sensing 27:1297-1328

Malvern Panalytical a Spectris Company (n.d) ASD FieldSpec range. https://www.malvernpanalytical.com/en/products/product-range/asd-range/fieldspec-range?campaignid=1564620399&adgroupid=59275649036&creative=603696200154&keyword=fieldspec4&matchtype=e&network=g&device=c&gclid=Cj0KCQjwyOuYBhCGARIsAIdGQRPblK646BdxXB8VjEF2e9i7UqghWpPo5p2gW2om9H7-cTgWAZx4sOAaAmmyEALw_wcB (accessed 01 July 2022)

Mongolian Statistical Information Service (2022) Livestock. https://1212.mn/Stat.aspx?LIST_ID=976_L10_1&type=tables (accessed 20 August 2022)

Musande V, Kumar A, Kale K (2012) Cotton crop discrimination using fuzzy classification approach. Journal of the Indian Society of Remote Sensing 40:589-597

NAMEM, MEGDT (2015) Монгол орны бэлчээрийн төлөв байдлын тайлан 2015 [National report on the rangeland health of Mongolia 2015]. Selenge press, Ulaanbaatar.

https://www.eda.admin.ch/dam/countries/countries-content/mongolia/en/Mongolia-Rangeland-Health-Report_MN.pdf (in Mongolian)

NASA (n.d.) What is the remote sensing? https://www.earthdata.nasa.gov/learn/backgrounders/remote-sensing (accessed 10 July 2022)

Petz K, Alkemade R, Bakkenes M, Schulp CJE, Velde MVD, Leemans R (2014) Mapping and modelling trade-offs and synergies between grazing intensity and ecosystem services in rangelands using global-scale datasets and models. Global Environmental Change 29:223–234

Phiri D, Simwanda M, Salekin S, Nyirenda VR, Murayama Y, Ranagalage M (2020) Sentinel-2 data for land cover/use mapping: A review. Remote Sensing 12:1-36

Qi J, Chehbouni A, Huete AR, Kerr YH, Sorooshian S (1994) A modified soil adjusted vegetation index. Remote Sensing of Environment 48:119-126

Rouse JW, Haas RH, Schell JA, Deering DW (1974) Monitoring vegetation systems in the great plains with ERTS. Pages 309-317. In: Freden SC, Mercanti EP, Becker MA (eds.) Third Earth Resources Technology Satellite-1 Symposium. Volume 1: Technical presentations, section A. Proceedings of a symposium held by Goddard Space Flight Center, Washington DC, 10-14 December 1973. NASA, Washington, DC

Roy PS (1989) Spectral reflectance characteristics of vegetation and their use in estimating productive potential. Proceeding /Indian Academy of Sciences 99:59-81

Scotford IM, Miller PCH (2005) Applications of spectral reflectance techniques in northern European cereal production: A review. Biosystems Engineering 90:235-250

Thornton PK (2010) Livestock production: recent trends, future prospects. Philosophical Transactions of the Royal Society B. Biological Sciences 365:2853-2867

Tucker CJ (1979) Red and photographic infrared linear combinations for monitoring vegetation. Remote Sensing of Environment 8:127–150

Wikum DA, Shanholtzer GF (1978) Application of the Braun-Blanquet cover-abundance scale for vegetation analysis in land development studies. Environmental Management 2:323-329

Wolf J, Chen M, Asrar GR (2021) Global rangeland primary production and its consumption by Livestock in 2000–2010. Remote Sensing 13:1-23

Yunatov AA (1976) Бүгд найрамдах Монгол ард улсын ургамлын нөмрөгийн үндсэн шинжүүд [Fundamental characteristics of vegetation of the Mongolian People's Republic] Government printing office, Ulaanbaatar (in Mongolian)

APPENDICES

Appendix I. Sentinel-2 MSI sampling data of 69 field plots in 2021.

No	B2	B3	B4	B8	NDVI	DVI	MSAVI	EVI	Wet biomass	Dried biomass
1	454.5	760	635	2555	0.6028	0.1899	0.7521	0.3677	161.71	107.42
2	443.5	757.5	615	2627	0.6196	0.1974	0.7651	0.3848	194.2	89.91
3	509	803	682	2544	0.5064	0.1707	0.6723	0.3309	126.6	36
4	485	780	648	2596	0.5131	0.1728	0.6781	0.3359	54.4	25
5	458	756	573	2664	0.5531	0.1856	0.7122	0.3609	132	31.4
6	306	655	353	3642	0.8151	0.3271	0.8981	0.5738	61.7	23
7	308	590	386	3196	0.7388	0.2716	0.8498	0.4707	136.6	46
8	352	602	436	2670	0.6476	0.2099	0.7861	0.3928	126	47.5
9	338	619	430	2656	0.6553	0.2103	0.7918	0.3982	78.1	29
10	550	828	855	2542	0.4603	0.1627	0.6304	0.2932	239.8	92
11	548	814	824	2592	0.4904	0.1705	0.6581	0.3112	215.8	90
12	511	768	698	2446	0.5232	0.1668	0.6869	0.3235	130.7	52
13	511	762	719	2622	0.5491	0.1843	0.7089	0.3472	169.8	70.1
14	587	848	751	2840	0.5403	0.1976	0.7015	0.3752	115.3	62
15	609	873	785	2820	0.5246	0.1938	0.6882	0.3649	152.8	83
16	717	1178	1572	2744	0.2627	0.1062	0.4161	0.1648	53.25	38
17	726	1198	1562	2686	0.2651	0.1068	0.4191	0.1665	87.13	67
18	510	807	808	2312	0.4515	0.1330	0.6220	0.2557	96.21	68
19	697	1212	1360	3204	0.3961	0.1734	0.5674	0.2751	159.25	96
20	838	1334	1656	3182	0.3116	0.1412	0.4751	0.2178	116.13	62
21	821	1396	1694	3222	0.2900	0.1356	0.4496	0.2024	92.26	53
22	717	1220	1410	3212	0.3839	0.1732	0.5547	0.2719	147.25	86
23	378	620	493	2490	0.5638	0.1801	0.7210	0.3418	110	92
24	406	659	592	2208	0.4735	0.1468	0.6427	0.2775	157.1	93.5
25	861.5	1264	1394	2687	0.2979	0.1183	0.4590	0.2090	225.18	86
26	485	804.5	731	2631	0.5363	0.1746	0.6982	0.3289	313.2	144.5
27	512	797.5	786.5	2483	0.4888	0.1572	0.6566	0.2920	183.6	82.5
28	491	800	682	2644	0.5999	0.2069	0.7499	0.3920	200.5	104.8
29	526	839	767	2790	0.5710	0.2063	0.7269	0.3852	112.6	52
30	568	905	803	2778	0.5615	0.2104	0.7191	0.3901	108.8	52.5
31	586	925	829	2684	0.5421	0.1958	0.7030	0.3666	117.5	55.2
32	580	915	1070	2588	0.4061	0.1463	0.5775	0.2531	227.63	87
33	749.5	1157	1397	2594	0.3050	0.1204	0.4673	0.1962	87	59
34	786.5	1210	1457	2734	0.3168	0.1302	0.4811	0.2090	79	62.3
35	734.5	1115	1337	2592	0.3285	0.1270	0.4945	0.2119	74.9	48.5
36	720	1058	1256	2614	0.3272	0.1218	0.4931	0.2084	63.4	34.5
37	747	1066	1256	2598	0.3470	0.1284	0.5152	0.2260	72.5	68.2
38	697	1038	1208	2542	0.3696	0.1372	0.5397	0.2383	68.6	33
39	689	1011	1338	2226	0.2626	0.0926	0.4159	0.1549	45.5	30.5
40	390	690	547	2580	0.5775	0.1859	0.7321	0.3256	77	25
41	262	496	339	2666	0.6883	0.2146	0.8153	0.3790	65	21
42	601	929	1086	2458	0.3498	0.1274	0.5183	0.2089	82	38

43	544.5	843.5	871	2516	0.4339	0.1524	0.6052	0.2764	81	42
44	399.5	650.5	574.5	2346	0.5928	0.1840	0.7443	0.3225	71	33
45	685	993	1100	2618	0.3613	0.1394	0.5308	0.2389	143.6	61
46	443	678	609	2302	0.4918	0.1521	0.6593	0.2920	141	59
47	529	818	780	2600	0.4999	0.1711	0.6666	0.3173	143.6	61
48	681	909	966	2548	0.4133	0.1495	0.5849	0.2740	169.8	70.1
49	653	1021	1204	2412	0.3019	0.1064	0.4638	0.1844	43.1	30
50	659	1056	1242	2536	0.3330	0.1240	0.4995	0.2075	88	65
51	608	990	1178	2596	0.3577	0.1312	0.5269	0.2187	86	60
52	674	1088	1306	2518	0.2993	0.1080	0.4607	0.1789	95	59
53	398	804	755	2690	0.5558	0.1922	0.7145	0.3462	94	63
54	400	775	762	2666	0.5491	0.1890	0.7089	0.3430	90	62
55	812	1360	1538	3022	0.3268	0.1408	0.4926	0.2276	91	62.9
56	452	828	836	2612	0.5151	0.1776	0.6799	0.3191	93	63.5
57	412	693	590	2468	0.4937	0.1694	0.6610	0.3088	157.1	93.5
58	519	785.5	740.5	2334	0.4411	0.1373	0.6121	0.2649	33	18
59	470.5	758	694.5	2495.5	0.5331	0.1586	0.6954	0.3069	34	17.5
60	622.5	922.5	1021	2291	0.3747	0.1249	0.5451	0.2278	140.5	49
61	561	875	741	2784	0.5963	0.2195	0.7471	0.4157	101	67.5
62	743.5	1082.5	1258	2501	0.3676	0.1272	0.5376	0.2277	75	45
63	501.5	816	705	3271	0.6512	0.2584	0.7887	0.4713	77	61
64	559	912	1102	2414	0.3662	0.1248	0.5360	0.2135	65.3	40.5
65	470.5	766	638	2646	0.6053	0.1957	0.7541	0.3797	190	50
66	695	1010	1196	2478	0.3501	0.1284	0.5185	0.2226	55.3	35.5
67	738	1036	1154	2702	0.3963	0.1502	0.5676	0.2700	40.5	30.1
68	613	933	965	2850	0.5091	0.1923	0.6747	0.3480	71	34
69	466.5	760	644	2594	0.6052	0.1913	0.7540	0.3742	189	70

Appendix II. Portable spectroradiometer sampling data of 39 field plots in 2021.

No	**Blue**	**Green**	**Red**	**NIR**	**NDVI**	**DVI**	**MSAVI**	**EVI**	**Wet biomass**	**Dried biomass**
1	0.0268	0.0649	0.0377	0.2677	0.7530	0.2300	0.4080	0.4445	161.71	107.42
2	0.0249	0.0638	0.0345	0.2666	0.7707	0.2321	0.4151	0.4507	194.2	89.91
3	0.0485	0.0959	0.0725	0.2904	0.6003	0.2179	0.3557	0.3999	126.6	36
4	0.0466	0.0821	0.0664	0.3459	0.6781	0.2795	0.4503	0.5011	54.4	25
5	0.0390	0.0607	0.0557	0.3122	0.6971	0.2565	0.4291	0.4736	132	31.4
6	0.0331	0.0703	0.0450	0.4247	0.8083	0.3797	0.6154	0.6561	61.7	23
7	0.0151	0.0666	0.0176	0.1586	0.7998	0.1409	0.2689	0.3061	136.6	46
8	0.0230	0.0695	0.0352	0.2895	0.7834	0.2544	0.4510	0.4789	126	47.5
9	0.0230	0.0807	0.0330	0.1802	0.6901	0.1472	0.2699	0.3051	78.1	29
10	0.0432	0.0790	0.0598	0.3133	0.6796	0.2536	0.4205	0.4703	239.8	92
11	0.0349	0.0846	0.0496	0.3415	0.7462	0.2919	0.4889	0.5298	215.8	90
12	0.0308	0.0779	0.0474	0.3397	0.7553	0.2923	0.4927	0.5249	130.7	52
13	0.0565	0.0792	0.0802	0.2968	0.5747	0.2167	0.3478	0.4001	169.8	70.1
14	0.0510	0.0815	0.0787	0.3210	0.6063	0.2423	0.3858	0.4296	115.3	62

15	0.0516	0.1082	0.0884	0.3102	0.5565	0.2218	0.3489	0.3814	152.8	83
16	0.0808	0.1092	0.1625	0.3117	0.3145	0.1491	0.2112	0.2219	53.25	38
17	0.0825	0.0968	0.1387	0.3233	0.3996	0.1846	0.2678	0.3003	87.13	67
18	0.0825	0.1150	0.1387	0.3233	0.3996	0.1846	0.2678	0.3003	96.21	68
19	0.0596	0.1047	0.1041	0.3774	0.5675	0.2732	0.4048	0.4393	159.25	96
20	0.1025	0.1166	0.1872	0.4277	0.3911	0.2405	0.3115	0.3373	116.13	62
21	0.0507	0.0834	0.0891	0.2322	0.4454	0.1431	0.2323	0.2581	92.26	53
22	0.0776	0.0925	0.1362	0.3347	0.4216	0.1985	0.2873	0.3162	147.25	86
23	0.0516	0.0748	0.0806	0.3636	0.6372	0.2830	0.4397	0.4847	110	92
24	0.0469	0.0820	0.0790	0.2888	0.5703	0.2097	0.3386	0.3716	157.1	93.5
25	0.0302	0.0320	0.0434	0.2719	0.7247	0.2285	0.3993	0.4374	225.18	86
26	0.0357	0.0499	0.0563	0.3010	0.6851	0.2448	0.4110	0.4463	313.2	144.5
27	0.0341	0.0472	0.0506	0.2842	0.6976	0.2336	0.3997	0.4384	183.6	82.5
28	0.0379	0.0771	0.0557	0.2607	0.6479	0.2050	0.3500	0.3909	200.5	104.8
29	0.0494	0.0685	0.0723	0.2898	0.6009	0.2176	0.3555	0.4021	112.6	52
30	0.0423	0.0607	0.0611	0.3030	0.6643	0.2418	0.4016	0.4470	108.8	52.5
31	0.0460	0.0850	0.0652	0.3417	0.6794	0.2764	0.4473	0.4978	117.5	55.2
32	0.0514	0.0834	0.0785	0.3001	0.5855	0.2217	0.3564	0.4000	227.63	87
33	0.0540	0.0819	0.0988	0.2208	0.3815	0.1219	0.1957	0.2164	87	59
34	0.0543	0.1159	0.0983	0.2205	0.3833	0.1222	0.1963	0.2177	79	62.3
35	0.0803	0.1166	0.1458	0.2657	0.2913	0.1199	0.1770	0.1948	74.9	48.5
36	0.0852	0.1057	0.1223	0.2978	0.4178	0.1755	0.2635	0.3151	63.4	34.5
37	0.0775	0.1537	0.1119	0.2472	0.3767	0.1353	0.2108	0.2528	72.5	68.2
38	0.0898	0.0764	0.1474	0.2955	0.3344	0.1481	0.2153	0.2459	68.6	33
39	0.0838	0.1155	0.1237	0.2625	0.3596	0.1389	0.2114	0.2523	45.5	30.5

Appendix III. Portable spectroradiometer sampling data of 10s field plots in 2022.

No	NIR	RED	BLUE	NDVI	DVI	MSAVI	EVI	Wet biomass	Dried biomass
1	0.3067	0.0551	0.0368	0.6952	0.2515	0.4224	0.4619	188.53	81.63
2	0.3060	0.0552	0.0368	0.6944	0.2508	0.4212	0.4607	163.72	104.57
3	0.4019	0.0535	0.0360	0.7649	0.3483	0.5603	0.5992	186.05	134.23
4	0.5063	0.0421	0.0334	0.8463	0.4641	0.7159	0.7691	379.66	108.92
5	0.3053	0.0553	0.0368	0.6935	0.2501	0.4201	0.4594	292.19	85.49
6	0.3124	0.0567	0.0378	0.6928	0.2557	0.4270	0.4670	136.05	93.12
7	0.4913	0.0504	0.0341	0.8141	0.4410	0.6738	0.7169	207.62	118.23
8	0.3855	0.0554	0.0441	0.7489	0.3302	0.5337	0.5950	255.39	81.63
9	0.5222	0.0297	0.0222	0.8922	0.4925	0.7773	0.8027	248.20	97.79
10	0.6111	0.0413	0.0339	0.8734	0.5698	0.8030	0.8875	242.49	115.32

Appendix IV. Template of record for plant researching.

Plant record sheet №

Province name: _____ Soum name: _____
Professional body name: _____
Date of record: _____ year _____ month _____ day
Monitoring plot number: _____ Sampling number: _____
Geographic name: _____
Characteristic of soil: _____
Surface: A. Aspect _____ degree of slope _____
B. Flat, convex, concave, side of the mountain and mountain ridge
Geographical coordinates: N _____, E _____, H _____
Type name: _____
Vegetation cover: weeds ____%, bare_____%, rock ____%, litter _____%, shrub ____%, gravel _____%, sand _____%, other _____%,
Wet biomass _____, dried biomass _____,
Area of field sampling _____ m^2 / cm^2, summer condition _____,
Animal effect _____.

№	Name of plant	Cover, %	Height, cm	Stages of plant growth	Notes
	Number of species _____ in 1m^2, _____ in 100m^2 Community_____	Grass_____%, legume _____%, sedge _____%, forb _____%, artemisia _____%, onion _____%, invader _____%.			

Field sampling condition /to explain/

Condition type	Field cover, %	Distribution	Size /diameter, height and depth/	Notes

Degree of effect /to explain/

Monitoring plot number	Degree of effect /severity, moderate, weak/						
	Abiotic	Pest rodent	Polluted	Degraded	Sand migration	Water erosion	Gully